Linear-Scaling Self-Consistent Field Theory Based Molecular Dynamics: Application to C_{60}-Buckyballs Colliding with Graphite

D. Richters, T. D. Kühne

published in

NIC Symposium 2018
K. Binder, M. Müller, A. Trautmann (Editors)

Forschungszentrum Jülich GmbH,
John von Neumann Institute for Computing (NIC),
Schriften des Forschungszentrums Jülich, NIC Series, Vol. 49,
ISBN 978-3-95806-285-6, pp. 155.
http://hdl.handle.net/2128/17544

Linear-Scaling Self-Consistent Field Theory Based Molecular Dynamics: Application to C_{60}-Buckyballs Colliding with Graphite

Dorothee Richters[1] **and Thomas D. Kühne**[2,3]

[1] Institute of Physical Chemistry and Center of Computational Sciences, Johannes Gutenberg University Mainz, Staudinger Weg 9, 55128 Mainz, Germany
E-mail: d.richters@uni-mainz.de

[2] Dynamics of Condensed Matter and Center for Sustainable Systems Design, Department of Chemistry, University of Paderborn, Warburger Str. 100, 33098 Paderborn, Germany

[3] Paderborn Center for Parallel Computing and Institute for Lightweight Design with Hybrid Systems, University of Paderborn, Warburger Str. 100, 33098 Paderborn, Germany
E-mail: tdkuehne@mail.upb.de

In this work, we investigate the collision of a C_{60} fullerene with graphite using large-scale molecular dynamics simulations, where the interatomic forces are computed "on-the-fly" by means of self-consistent tight-binding calculations. This method is based on an exact decomposition of the grand-canonical potential for independent fermions suitable for linear-scaling electronic structure calculations. We observe that at lower collision velocities, the buckyball is rebound from the graphite surface, but that starting from 50 km/s chemisorption processes are occurring that causes the buckyball to stick to the topmost graphene layer.

1 Introduction

Ab initio molecular dynamics (AIMD) is a very powerful computational method for simulating the complex interplay between electrons and protons at finite temperature, which makes up atoms[1–3]. To that extend, the real-time evolution of the atoms is computed by solving Newton's equations of motion, whereas the intermolecular forces are calculated "on-the-fly" by parameter-free electronic structure calculations. At variance to conventional MD simulations based on empirical interaction potentials, the increased accuracy and in particular its transferability and therefore predictive power of this approach are among the key advantages of AIMD. As a consequence, its application ranges from chemistry and physics over material sciences and nanotechnology to biophysics and biology, just to name a few[4].

However, even the *ab initio* approach is not without problems: the significant computational cost has to be carefully balanced against system size and sampling requirements. For this reason, effective single-particle theories such as Hartree-Fock, density functional theory and semi-empirical tight-binding are still the most commonly employed electronic structure methods within AIMD[3,4]. All of these techniques share the same computational requirement to diagonalise a very large Hamilton matrix in every time step to compute the total energy and particularly the nuclear forces. The associated computational effort scales as $\mathcal{O}(N^3)$, where N denotes the number of atoms. Hence, the development of alternative methods that scales only linearly with respect to N would be very desirable, thus making a large variety of systems accessible to AIMD that previously were thought to be

not feasible. In fact, several so-called linear-scaling techniques have been proposed to circumvent the conventionally cubic scaling matrix diagonalisation[5–11]. But in spite of recent progress[12–15], the critical system sizes after which these schemes become favourable is still rather large, in particular for metallic systems and/or if high accuracy is required.

For this purpose, recently an improved field-theoretic approach has been proposed[16], which is based on an exact decomposition of the grand-canonical potential (GCP) for independent fermions and does neither rely on the ability to localise the orbitals, nor that Hamilton matrix is well-conditioned[17,18]. Instead, the finite-temperature density matrix, or Fermi matrix, is obtained by an hybrid approach that combines Chebyshev polynomial expansion and iterative inversion techniques[18,19], and therefore allows for linear system size scaling even for metallic systems[16]. The inherent energy drift of AIMD simulations, arising from truncation errors and incomplete convergence of the self-consistent field (SCF) cycle, is compensated by means of a properly modified Langevin equation[3,21,22]. In order to reconcile the resilience of C_{60} fullerene-graphite collisions, a more accurate self-consistent tight-binding scheme (SCTB) that permits to realistically simulate reactive processes, such as breaking and making of chemical bonds, is employed here[23].

In this work, we demonstrate the predictive power of this approach using the example of buckyball collisions with graphite. Previously, using the Takai-Lee-Halicioglu-Tiller (TLHT) model potential[24], Man *et al.* demonstrated that for collision velocities between 38 and $69.5\ km/s$, the C_{60} fullerene is severely deformed, but regains its initial shape after scattering[25–27]. On the other hand, in a more recent non-self-consistent tight-binding study it was shown that C_{60} buckyballs and graphite are able to withstand impact velocities of up to $44\ km/s$, but also that from $54\ km/s$ on covalent bonds of the buckyball are irreversible broken. At even higher velocities of $57\ km/s$, also the topmost graphene layer exhibits defects, while beginning from $59\ km/s$ individual bonds with the substrate are emerging[28].

2 Linear Scaling Hybrid Approach to the Grand-Canonical Potential

We start with the generic expression for the total energy E of an effective single-particle theory

$$E = 2 \sum_{i=1}^{N_e/2} \varepsilon_i + V_{dc}, \tag{1}$$

where N_e is the number of electrons. The sum of the lowest $N_e/2$ doubly occupied eigenvalues ε_i of the Hamilton matrix $\mathbf{H}$ is referred to as band-structure energy, whereas V_{dc} accounts for double counting correction terms and the nuclear Coulomb repulsion. While it is well known how to compute V_{dc} with linear scaling computational effort, the complexity of determining all occupied orbitals by diagonalising $\mathbf{H}$ is $\mathcal{O}(N_e^3)$. Fortunately, Eq. 1 can be equivalently written as

$$E = Tr[\mathbf{PH}] + V_{dc}, \tag{2}$$

where $\mathbf{P}$ is the so-called one-particle density matrix. This is to say that the cubic scaling conventional matrix diagonalisation can be circumvented by directly calculating $\mathbf{P}$ instead of all the ε_i's.

For that purpose, we follow Alavi and coworkers and consider the following (Helmholtz) free energy functional[29]

$$\mathcal{F} = \Omega + \mu N_e + V_{dc}, \tag{3}$$

where μ is the chemical potential and Ω the GCP for non-interacting fermions

$$\Omega = -\frac{2}{\beta} \ln \det \left(\mathbf{I} + e^{\beta(\mu\mathbf{S}-\mathbf{H})} \right). \tag{4}$$

Here, $\beta^{-1} = k_B T_e$ defines the finite electron temperature, whereas $\mathbf{S}$ is the overlap matrix that is equal to the identity matrix $\mathbf{I}$ if and only if the orbitals are expanded in an orthonormal basis set. In the low-temperature limit

$$\lim_{\beta\to\infty} \Omega = 2 \sum_{i=1}^{N} \varepsilon_i - \mu N_e, \tag{5}$$

the band-structure energy is recovered and $\lim_{\beta\to\infty} \mathcal{F} = E$ holds.

As shown by Krajewski and Parrinello it is possible to factorise the operator of Eq. 4 into P terms[17]. Without any loss of generality we are assuming that P is even, so that

$$\begin{aligned} \mathbf{I} + e^{\beta(\mu\mathbf{S}-\mathbf{H})} &= \prod_{l=1}^{P} \left(\mathbf{I} - e^{\frac{i\pi}{P}(2l-1)} e^{\frac{\beta}{P}(\mu\mathbf{S}-\mathbf{H})} \right) \\ &= \prod_{l=1}^{P} \mathbf{M}_l = \prod_{l=1}^{P/2} \mathbf{M}_l^* \mathbf{M}_l, \end{aligned} \tag{6}$$

where the matrices $\mathbf{M}_l,\ l = 1, \ldots, P$ are defined as

$$\mathbf{M}_l := \mathbf{I} - e^{\frac{i\pi}{P}(2l-1)} e^{\frac{\beta}{P}(\mu\mathbf{S}-\mathbf{H})}, \tag{7}$$

while * denotes complex conjugation. From this it follows that the GCP can be expressed as

$$\begin{aligned} \Omega &= -\frac{2}{\beta} \ln \det \prod_{l=1}^{P} \mathbf{M}_l = -\frac{2}{\beta} \sum_{l=1}^{P/2} \ln \det \left(\mathbf{M}_l^* \mathbf{M}_l \right) \\ &= \frac{4}{\beta} \sum_{l=1}^{P/2} \ln \left(\det(\mathbf{M}_l^* \mathbf{M}_l) \right)^{-\frac{1}{2}}. \end{aligned} \tag{8}$$

As a consequence, all physical relevant observables can be directly obtained as functional derivatives of the GCP with respect to a suitable external parameter, e.g.

$$E = \lim_{\beta\to\infty} \mathcal{F} = 2 \sum_{i=1}^{N_e/2} \varepsilon_i + V_{dc} = \frac{\partial(\beta\Omega)}{\partial\beta} - \mu \frac{\partial\Omega}{\partial\mu} + V_{dc}, \tag{9}$$

where $-\partial\Omega/\partial\mu = N_e$. In particular, the Fermi matrix, which in the low-temperature limit is identical to $\mathbf{P}$, can be written as

$$\begin{aligned}\mathcal{P} = \frac{\partial\Omega}{\partial\mathbf{H}} &= \frac{4}{P}\sum_{l=1}^{P/2}\left(\mathbf{I} - \left(\mathbf{M}_l^*\mathbf{M}_l\right)^{-1}\right) \\ &= \frac{2}{P}\sum_{l=1}^{P/2}\left(\mathbf{I} - \mathrm{Re}\,\mathbf{M}_l^{-1}\right), \end{aligned} \tag{10}$$

where $\mathbf{S} = -\partial\mathbf{H}/\partial\mu$. Therefore,

$$\Omega = Tr[\mathcal{P}(\mathbf{H} - \mu\mathbf{S})] \tag{11}$$

and similarly all physical observables can be expressed as the trace of a matrix product with $\mathcal{P}$.

The notion underlying this method is that $\mathcal{P}$, which at low temperature corresponds to the square of the wave function, can be decomposed into a sum of $\mathbf{M}_l^{-1}$ matrices, each at higher effective temperature β/P. Thus, not only $\mathbf{M}_l^{-1}$ is throughout much sparser than $\mathcal{P}$[18,19], but moreover the Maxwell-Boltzmann distribution becomes eventually valid. Exploiting the latter, it is much more convenient to invert $P/2$ matrices that except for very few are all very sparse, instead of diagonalising a single matrix $\mathbf{H}$, which typically is rather dense. Specifically, just a handful of $\mathbf{M}_l$ matrices, where l is close to $P/2$, are ill-conditioned and only for them the calculation of $\mathbf{M}_l^{-1}$ is computational significant. All other $\mathbf{M}_l$ matrices are very well-conditioned and can be efficiently inverted by a Chebychev expansion at inessential computational cost[18,19]. These complementary properties immediately suggest the following hybrid approach: At first, an optimal $\bar{l}$ is chosen and all $\mathbf{M}_l$ matrices with $l < \bar{l}$ are inverted by a Chebyshev polynomial expansion, while for $l \geq \bar{l}$ the inversion is performed by a Newton-Schulz iteration. The optimal value of $\bar{l}$ can be found by minimising an *a priori* estimate of the total number of matrix multiplications[18,19]. In general, $P/2 - \bar{l}$ is relatively small and depends only weakly on β, so that just a few $\mathbf{M}_l$ matrices are inverted using the Newton-Schulz iteration, regardless of the electronic temperature. As said, the Chebychev polynomial expansion is essentially independent of P and computational negligible.

3 Computational Details

For our simulations we have employed the SCTB model for hydrocarbons by Horsfield *et al.*[20], as implemented in the CMPTool code [a]. All of the calculation have been performed in the canonical NVT ensemble by means of the modified Langevin equation using a discretised time step of 0.5 fs. The convergence threshold of the SCF loop to enforce LCN was set to $\Delta q_{\max} = 0.05$. The decomposition of Eq. 10 was realised using $P = 10000$. The minimisation of the required matrix multiplications with respect to $\bar{l}$ yields $\bar{l} = P/2 - 2$. This is to say that except for two, all matrices can be inverted by a Chebyshev polynomial expansion with an estimated length, which corresponds to the degree of the polynomial, of $m_C(\bar{l}) \leq 61$. As the optimisation with respect to $\bar{l}$ is only an approximation, we increase the overall efficiency by choosing $\bar{l} = P/2 - 4$ which entails $m_C(\bar{l}) \approx 30$.

[a] See `https://cmsportal.caspur.it/index.php/CMPTool` for further information.

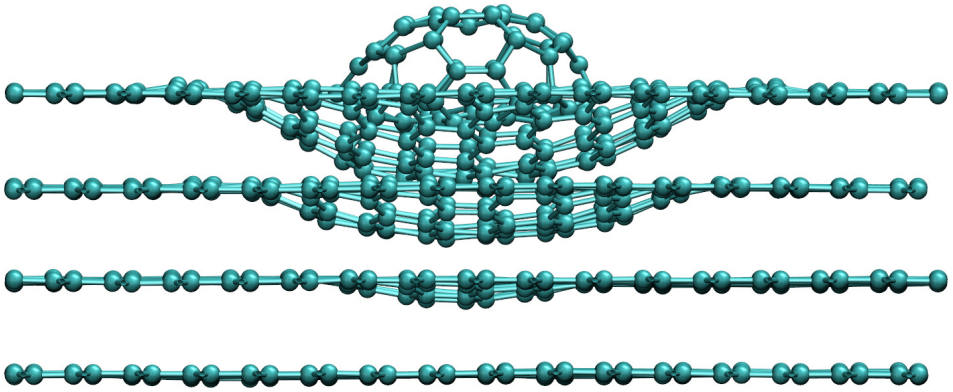

Figure 1. Buckyball colliding with the graphite surface at $v = 30\ km/s$. Although the C_{60} fullerene is severely deformed, no covalent bonds are broken.

We have considered graphite made up of four graphene layers in a simulation cell of size $34.43 \times 34.08 \times 100$ Å^3 with periodic boundary conditions. From above the topmost graphene layer, an initially 15.0 Å distanced C_{60} fullerene is shot onto the graphite surface. In total five simulations each consisting of 1852 carbon atoms are conducted, where the impact velocities of the buckyball were initialised to 30, 40, 50 and 60 km/s, respectively.

4 Results and Discussion

As can be seen in Figs. 1 and 2, if the C_{60} fullerene hits the graphite surface with $v = 30\ km/h$, which is the smallest collision velocity we have considered, the buckyball is severely deformed, but regains its original shape while bouncing back from the graphene layers. The topmost graphene layers are also deformed and compressed, but no breaking of bonds is observed. The rather strong flexibility of the graphene layers is due to the rather weak London dispersion interactions between the layers and the strong sp^2-bonding in-plane that permits to absorb the rather high kinetic energy of the C_{60} fullerene unharmed. At $v = 40\ km/s$, however, the impact causes that individual bonds of the buckyball and the topmost graphene layer are broken. Yet, as soon as the C_{60} fullerene bounces back, the fleetingly broken bonds of the topmost graphene layer immediately recover. As is visible in Fig. 3, the buckyball itself is compressed to such an extend that the truncated icosahedron structure is destroyed. Upon repulsion, the buckyball mostly restores itself, though a few defects, which can be recognised in Fig. 4, remain.

In contrast to the lower shooting velocities, at $v = 50\ km/s$, we not only observe covalent bond breaking within the C_{60} fullerene, as well as the topmost graphene layer, but also the formation of new bonds that are strong enough to prevent the detachment of the C_{60} fullerene. This is a manifestation of the fact that the kinetic energy scale is tiny in comparison to that of covalent bonding. In any case, due to the covalent bonding of the buckyball to the topmost graphene layer, the latter can no longer recover and irreversible defects are emerging, as is shown in Fig. 5. While the upper half of the C_{60} fullerene is able to recover keeping the five-and-six-membered ring-structure intact, the lower part forms bonds

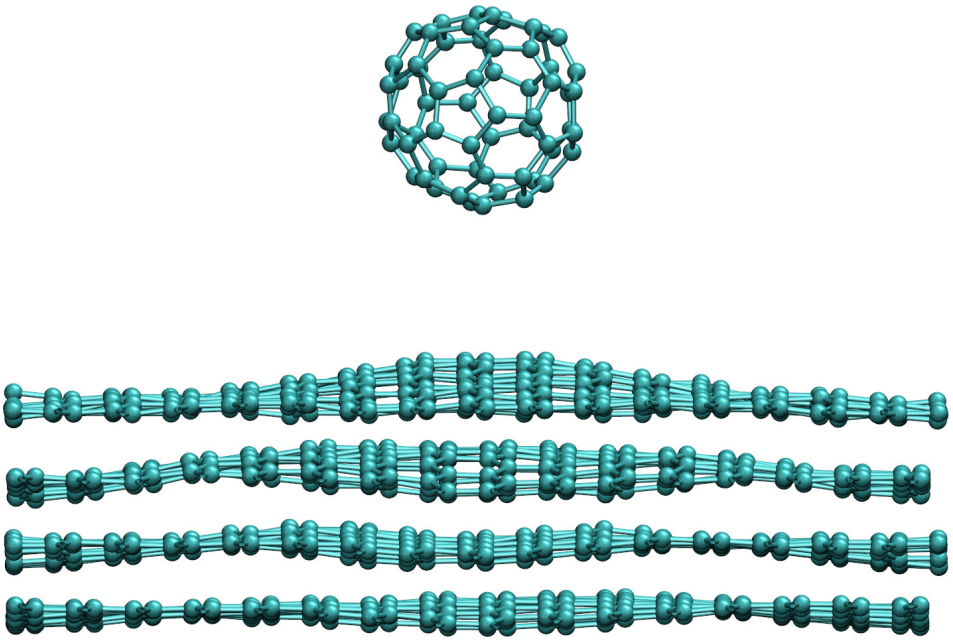

Figure 2. After the collision with $v = 30\ km/s$, the buckyball bounces back from the graphite surface and regains its original shape.

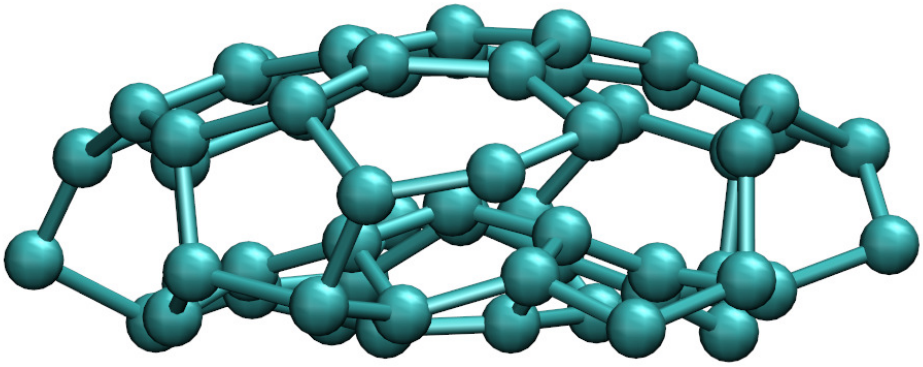

Figure 3. Detailed picture of the C_{60} fullerene when it hits the graphite surface at $v = 40\ km/s$. Even though no carbon atom is knocked out of the buckyball, its truncated icosahedron structure is temporarily destroyed.

with the destroyed graphene layer, making it a reactive collision process. This is in stark contrast with previous studies based on the classical TLHT[24–27], but in excellent agreement with more recent non-self-consistent tight-binding simulations[28]. This demonstrates the importance of explicitly incorporating bond breaking and making processes within the simulations.

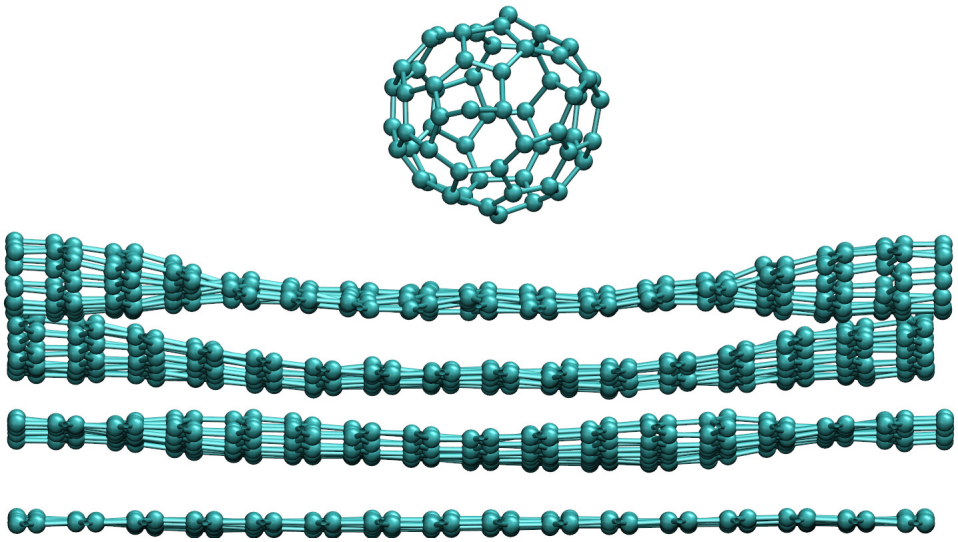

Figure 4. After the collision with $v = 40\ km/s$, the C_{60} fullerene rebounds from the graphite surface. Even though the topmost graphene layer and the buckyball mostly recovers itself, individual defects are remaining.

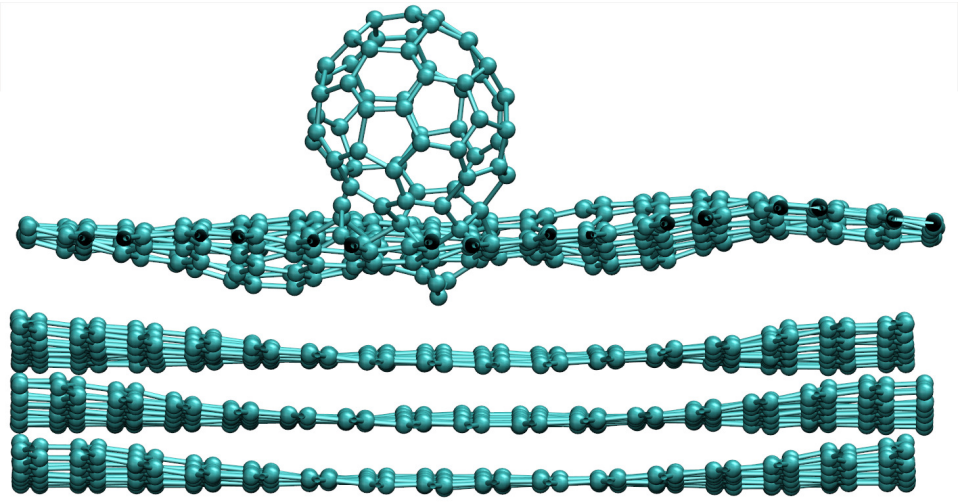

Figure 5. During the collision process with $v = 50\ km/s$, chemisorption processes are taking place that eventually causes the buckyball to sticks to the graphite surface.

Similar to the case with $v = 50\ km/s$, at $v = 60\ km/s$, covalent bond breaking can be observed at the graphite surface, as well as within the buckyball, which is destroyed and forms new bonds with the graphene layer. As displayed in Fig. 6, these chemisorption processes entails that the C_{60} fullerene sticks to the graphite surface. As before, only the

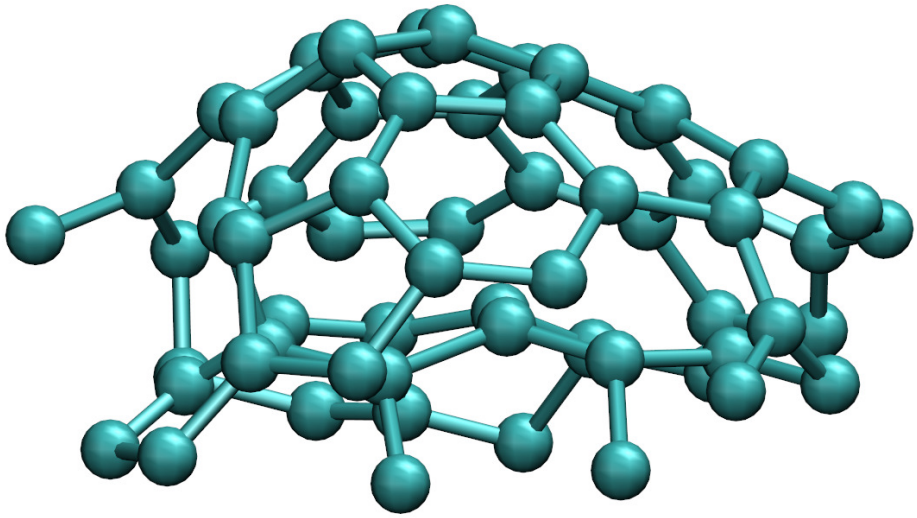

Figure 6. Detailed picture of the C_{60} fullerene after the collision at $v = 60\ km/s$ with the graphite surface. Only in the upper half the general hexagon/pentagon structure remains intact, while the lower part is bonded to the topmost graphene layer.

upper half of the buckyball made of hexagons and pentagons is still intact, the lower part is bonded to the graphene sheet. Even though all of this is very good agreement with experimental measurements, the latter indicates that the C_{60} fullerenes are stable up to collision energies of 250 eV, which corresponds to $v = 70\ km/s$[30,31]. Similarly, at this impact velocity, transient chemisorption processes that eventually causes the buckyballs to sticks to the graphite surface have been observed[32].

5 Conclusion

To summarise, using the recently proposed improved field-theoretic approach to the GCP for independent fermions[16,18,19], we have conducted large-scale SCTB-MD calculations to investigated the behaviour of a C_{60} fullerene colliding with graphite at different impact velocities. At variance to previous works, the main advantage of the present scheme is that bond breaking and making processes are explicitly taken in to account by means of linear-scaling electronic structure calculations.

Employing this technique, we found that till $v = 40\ km/s$, the buckyball and the graphite surface are both rather heavily deformed, but able to regain their original structure. Yet, starting at $v = 50\ km/s$, we observe chemisorption processes causing the C_{60} fullerene to stick on the graphite surface. During that process the distortions of the buckyball and the graphite surface are so severe that covalent bonds are irreversible broken. Even though this is in stark contrast with classical MD studies[25–27], it is in qualitatively good agreement with non-self-consistent tight-binding simulations[28], as well as experimental measurements[30–32].

Acknowledgements

Financial support from the Graduate School of Excellence MAINZ and the IDEE project of the Carl Zeiss Foundation is kindly acknowledged. Moreover, we would like thank the Gauss Centre for Supercomputing (GCS) for providing computing time through the John von Neumann Institute for Computing (NIC) on the GCS share of the supercomputer JUQUEEN at the Jülich Supercomputing Centre (JSC). This project has received funding from the European Research Council (ERC) under the European Union's Horizon 2020 research and innovation programme (grant agreement No 716142).

References

1. D. Marx and J. Hutter, *Ab Initio Molecular Dynamics*, Cambridge University Press, Cambridge, UK, 2009.
2. J. Hutter, *Car-Parrinello molecular dynamics*, WIREs Comput. Mol. Sci. **2**, 604, 2012.
3. T. D. Kühne, *Second generation Car-Parrinello molecular dynamics*, WIREs Comput. Mol. Sci. **4**, 391, 2014.
4. M. Parrinello, *From silicon to RNA: The coming of age of ab initio molecular dynamics*, Solid State Commun. **102**, 107, 1997.
5. S. Baroni and P. Giannozzi, *Towards Very Large-Scale Electronic-Structure Calculations*, Europhys. Lett. **17**, 547, 1992.
6. W. Yang, *Direct Calculation of Electron Density in Density-Functional Theory*, Phys. Rev. Lett. **66**, 1438, 1991.
7. G. Galli and M. Parrinello, *Large Scale Electronic Structure Calculations*, Phys. Rev. Lett. **69**, 3547, 1992.
8. X.-P. Li, R. W. Nunes, and D. Vanderbilt, *Density-matrix electronic-structure method with linear system-size scaling*, Phys. Rev. B **47**, 10891, 1993.
9. A. H. R. Palser and D. E. Manolopoulos, *Canonical purification of the density matrix in electronic-structure theory*, Phys. Rev. B **58**, 12704, 1998.
10. S. Goedecker, *Linear scaling electronic structure methods*, Rev. Mod. Phys. **73**, 122, 1994.
11. D. R. Bowler and T. Miyazaki, $\mathcal{O}(N)$ *methods in electronic structure calculations*, Rep. Prog. Phys. **75**, 036503, 2012.
12. N. D. M. Hine, M. Robinson, P. D. Haynes, C.-K. Skylaris, M. C. Payne, and A. A. Mostofi, *Accurate ionic forces and geometry optimization in linear-scaling density-functional theory with local orbitals*, Phys. Rev. B **83**, 195102, 2011.
13. S. Mohr, L. E. Ratcliff, P. Boulanger, L. Genovese, D. Caliste, T. Deutsch, and S. Goedecker, *Daubechies wavelets for linear scaling density functional theory*, J. Chem. Phys. **140**, 204110, 2014.
14. M. Arita, D. R. Bowler, and T. Miyazaki, *Stable and Efficient Linear Scaling First-Principles Molecular Dynamics for 10000+ Atoms*, J. Chem. Theory Comput. **10**, 5419, 2014.
15. S. Mohr, L. E. Ratcliff, L. Genovese, D. Caliste, P. Boulanger, S. Goedecker, and T. Deutsch, *Accurate and efficient linear scaling DFT calculations with universal applicability*, Phys. Chem. Chem. Phys. **17**, 31360, 2015.

16. D. Richters and T. D. Kühne, *Self-consistent field theory based molecular dynamics with linear system-size scaling*, J. Chem. Phys. **140**, 134109, 2014.
17. F. R. Krajewski and M. Parrinello, *Stochastic linear scaling for metals and nonmetals*, Phys. Rev. B **71**, 233105, 2005.
18. M. Ceriotti, T. D. Kühne, and M. Parinello, *An efficient and accurate decomposition of the Fermi operator*, J. Chem. Phys. **129**, 024707, 2008.
19. M. Ceriotti, T. D. Kühne, and M. Parrinello, *A hybrid approach to Fermi operator expansion*, AIP Conf. Proc. **1148**, 658, 2009.
20. A. P. Horsfield, P. D. Godwin, D. G. Pettifor, and A. P. Sutton, *Computational materials synthesis. I. A tight-binding scheme for hydrocarbons*, Phys. Rev. B **54**, 15773, 1996.
21. F. R. Krajewski and M. Parrinello, *Linear scaling electronic structure calculations and accurate statistical mechanics sampling with noisy forces*, Phys. Rev. B **73**, 041105, 2006.
22. T. D. Kühne, M. Krack, F. R. Mohamed, and T. Deutsch, *Efficient and Accurate Car-Parrinello-like Approach to Born-Oppenheimer Molecular Dynamics*, Phys. Rev. Lett. **98**, 066401, 2007.
23. G. Seifert and J.-O. Joswig, *Density-functional tight binding – an approximate density-functional theory method*, WIREs Comput. Mol. Sci. **5**, 295, 1999.
24. T. Takai, C. Lee, T. Halicioglu, and W. A. Tiller, *A model potential function for carbon systems: clusters*, J. Phys. Chem. **94**, 4480, 1990.
25. Z. Y. Man, Z. Y. Pan, and Y. K. Ho, *The rebounding of $\{C60\}$ on graphite surface: a molecular dynamics simulation*, Phys. Lett. A **209**, 53, 1995.
26. Z. Y. Pan, Z. Y. Man, and M. Hou, *The scattering of low energy C_{60} on graphite (0001) surfaces*, Z. Phys. D **41**, 175, 1997.
27. Z. Y. Pan, Z. Y. Man, Y. K. Ho, J. Xie, and Y. Yue, *Energy dependence of C_{60}-graphite surfaces collisions*, J. Appl. Phys. **83**, 4963, 1998.
28. F. Yun-Tuan and L. Cheng-Lin, *Tight-binding molecular dynamics study of C_{60}-graphite collisions*, Chin. Phys. **9**, 581, 2000.
29. A. Alavi, J. Kohanoff, M. Parrinello, and D. Frenkel, *Ab Initio Molecular Dynamics with Excited Electrons*, Phys. Rev. Lett. **73**, 2599, 1994.
30. R. D. Beck, P. St. John, M. M. Alvarez, F. Diederich, and R. L. Whetten, *Resilience of all-carbon molecules C60, C70, and C84: a surface-scattering time-of-flight investigation*, J. Phys. Chem. **95**, 8402, 1991.
31. H.-G. Busmann, Th. Lill, B. Reif, and I.V. Hertel, *Collision induced fragmentation and resilience of scattered C60+ fullerenes*, Surface Science **272**, 146, 1992.
32. H.-G. Busmann, Th. Lill, B. Reif, I. V. Hertel, and H. G. Maguire, *Energy partition in collisions of C60+ ions with diamond (111) and graphite (0001) surfaces*, J. Chem. Phys. **98**, 7574, 1993.